Theoretical analysis of the transport critical-state ac loss in arrays of superconducting rectangular strips

Enric Pardo,[1] Alvaro Sanchez,[1] Du-Xing Chen,[2] and Carles Navau[1,3]
[1]*Grup d'Electromagnetisme, Departament de Física, Universitat Autònoma Barcelona, 08193 Bellaterra (Barcelona), Catalonia, Spain*
[2]*ICREA and Grup d'Electromagnetisme, Departament of Física, Universitat Autònoma de Barcelona, 08193 Bellaterra (Barcelona), Catalonia, Spain*
[3]*Escola Universitària Salesiana de Sarrià, Passeig Sant Joan Bosco 74, 08017 Barcelona, Catalonia, Spain*
(Received 2 February 2004; revised manuscript received 29 November 2004; published 25 April 2005)

We present a systematic theoretical study of current profiles, magnetic field lines, and hysteresis ac loss in linearly arranged arrays of rectangular superconducting strips subjected to a transport current. Results are obtained by means of numerical calculations assuming the critical-state model with a constant critical current density. Because finite filament thickness and magnetic coupling effects are considered, we can provide some useful hints as to how to arrange the filaments in order to reduce the ac loss in actual superconducting tapes.

DOI: 10.1103/PhysRevB.71.134517 PACS number(s): 74.25.Sv, 84.71.Mn

I. INTRODUCTION

Some of the important applications of superconductors are based on the possibility of having a high value of supercurrent transported through them. For hard type II superconductors, the energy loss when carrying a static transport supercurrent is very small but it can be significant when the current is alternating. The reduction of ac loss is of fundamental importance for the application of superconductors to actual ac electrical devices, such as power transmission cables, ac magnets, and transformers.[1–3]

In recent years, a lot of effort has been made in the production of high-temperature superconducting (HTS) composite conductors, which are made of a superconducting core with a multifilamentary structure and a normal-metal conducting sheath or substrate. The most common HTS composite conductors are Bi-2223/Ag tapes, coated YBCO conductors, and MgB_2 tapes and wires.[3,4] The understanding of ac loss in these multifilamentary conductors is not only useful to reduce the energy dissipation but also to characterize the superconductor material properties.[5,6] Moreover, the study of the ac loss for several magnetically interacted conductors is also useful for applications.[2,7–11]

The critical-state model[12,13] has been shown to be a useful tool to describe the ac loss of superconducting wires. The model assumes that the current density has a magnitude J_c wherever it is nonzero. It was first applied to analytically calculate the ac loss for simple geometries, such as a cylinder,[13] a circular tube, or an infinite slab.[14] In the early 1970s, Norris paved the way for some of the modern models by calculating the ac loss produced by a transport current in a thin strip and an elliptical cross-section wire.[15] Further theoretical advances and the discovery of HTS materials motivated the study of other interesting geometries, such as a cylinder with two concentric circular shells with different J_c (Ref. 16) and some multifilamentary geometries, like vertical and horizontal arrays of an infinite number of thin strips[17] or double thin strips.[18]

Apart from the mentioned analytical studies, some numerical models within the critical-state model have been developed to describe superconductors with transport current, like those from Norris,[19] Fukunaga *et al.*,[20–22] Däumling,[23] and Pardo *et al.*[24] These numerical methods restrict the calculation region to the superconducting volume only. The geometry investigated numerically was a rectangular strip with arbitrary thickness,[20,23,24] after which extensive work on multifilamentary tapes was done by Fukunaga *et al.*[21,22] An alternative approach to the critical-state model is to assume a certain $E(J)$ dependence as $E \propto (J/J_c)^n$, where E is the electrical field. An interesting model considering this assumption is that developed by Brandt[25] for superconducting strips in applied magnetic fields, extended for the transport current case by Rhyner[26] and Yazawa *et al.*[27] Again, this model requires numerical calculations inside the superconductor only. Other authors applied conventional finite-element techniques to multifilamentary tapes, such as Stavrev *et al.*[28]

In spite of all the extensive theoretical work done on ac loss, the magnetic coupling behavior between superconducting filaments has not been systematically studied. To cover this lack, in this work we present accurate numerical calculations and discussions of current distribution, magnetic field lines, and ac loss for matrix arrays of rectangular strips. The matrix arrangement is found in many actual tapes[22,29,30] and is a simple geometry to study for the interaction between different tapes.

The calculations are performed by a numerical model based on the critical-state model with a constant critical current density, which is presented in Sec. II. In Sec. III, we first present a systematic study of the magnetic interaction among rectangular strips in both horizontal and vertical arrays, and then we use such a study as a basis to understand the magnetic interaction in a matrix array. A comparison of the model results with both experimental data and simplified analytical models is presented in that section. Finally, we summarize our conclusions in Sec. IV.

II. MODEL

We consider a set of infinitely long superconducting rectangular strips of cross-sectional dimensions $2a \times 2b$ along

the horizontal x and vertical y axis, respectively. We study the case of regularly arranged strips in a matrix configuration of $n_{s,x} \times n_{s,y}$ $(1 \leqslant n_{s,x}, n_{s,y} \leqslant 9)$ strips with horizontal and vertical separations d_x and d_y, respectively.

The rectangular strips are connected to each other in parallel and fed by an ac current with amplitude I_m. Such a connection is usually found in a real superconducting tape with neither twisting nor resistive barriers thanks to the metallic matrix or substrate. We assume that the contribution of the metallic region to the loss is negligible in front of the hysteretic superconductor loss. This assumption is valid for enough low frequencies.[31]

In the following we present the numerical model used for calculating the current profiles, the magnetic field lines, and the ac loss.

A. Magnetic energy minimization

The calculations presented in this work are carried out by the magnetic energy minimization (MEM)[32,33] based on the critical-state model with a constant critical current density J_c. The MEM, developed for cylinders[32,34] and tapes[33,35,36] in the presence of magnetic fields can be extended to the transport case, as presented in this section.

The magnetic energy W per unit length of an infinitely long circuit with uniform cross section along the z axis is[37]

$$W = \tfrac{1}{2} \int_{S_{xy}} J(\mathbf{r}) A_J(\mathbf{r}) dS, \tag{1}$$

where S_{xy} refers to the whole xy plane, J is the current density, and A_J is the vector potential created by J, being both $\mathbf{J}$ and $\mathbf{A}_J$ parallel to the z axis. It follows from the gauge of $\boldsymbol{\nabla} \cdot \mathbf{A} = 0$ that

$$A_J(\mathbf{r}) = -\frac{\mu_0}{4\pi} \int_{S_{xy}} J(\mathbf{r}') \ln[(x-x')^2 + (y-y')^2] dS'. \tag{2}$$

In order to apply the MEM procedure to the transport case we consider a circuit consisting of two identical superconducting tapes (each of which may consist of several strips) carrying opposite current and separated a large distance D compared to their cross-sectional dimensions, as done by Carr.[38] We choose the origin of coordinates in the center of one tape, which carries a transport current I, and we center the returning tape at $(x,y) = (D,0)$. With this configuration and using the approximation of large D, we obtain from Eq. (2) that the vector potential in the tape at the origin is

$$A_J(\mathbf{r}) \approx A(\mathbf{r}) + \frac{\mu_0}{2\pi} I \ln D, \tag{3}$$

where the first term is the vector potential created by the tape at the origin and the second is that created by the returning tape. Considering that the vector potential in each tape has the same magnitude but opposite sign and inserting Eq. (3) into (1), we obtain that the magnetic energy of the circuit is

$$W = \int_S J(\mathbf{r}) A(\mathbf{r}) dS + \frac{\mu_0}{2\pi} I^2 \ln D, \tag{4}$$

being S the cross section of the tape at the origin. The second term of Eq. (4) is constant for a fixed current I, so that the only term in the energy per tape that has to be minimized to determine the current distribution is

$$W' \equiv \tfrac{1}{2} \int_S J(\mathbf{r}) A(\mathbf{r}) dS, \tag{5}$$

which we call internal energy. We notice that we obtain the same expression for W' if we consider that the current returns through a perfectly conducting shell at a large distance D, as done by Norris,[15] instead of an identical superconducting tape.

B. Physical grounds of magnetic energy minimization

In our previous papers about MEM, we assume that the actual supercurrent distribution minimizes the magnetic energy.[32] The energy and flux minimization in the critical state was independently studied by Prigozhin,[39,40] Badia *et al.*,[41] and Chaddah and co-workers.[42] In these works it was shown that supercurrent distribution is such that minimizes a certain functional, which is not always the magnetic energy. In the following we demonstrate that in the initial curve, minimizing this functional is equivalent to minimizing the magnetic energy provided that current density penetrates monotonically from the surface.

Following the notation of Prigozhin,[40] in the absence of an applied field the supercurrent at a certain time is such that minimizes the functional

$$\mathcal{F}[J] = \tfrac{1}{2} \int_S J(\mathbf{r}) A(\mathbf{r}) dS - \int_S J(\mathbf{r}) \hat{A}(\mathbf{r}) dS, \tag{6}$$

with the constrains $\int_S J(\mathbf{r}) dS = I$ and $|J| \leqslant J_c$, being $\hat{A}$ the vector potential created by the supercurrent at the previous time layer, $\hat{J}$. The principle of minimization of this functional is found from first principles in Refs. 39 and 40. Defining the current density variation $\delta J \equiv J - \hat{J}$, we obtain from Eqs. (6) and (2) that

$$\mathcal{F}[\delta J + \hat{J}] = \tfrac{1}{2} \int_S \delta J(\mathbf{r}) \delta A(\mathbf{r}) dS - \tfrac{1}{2} \int_S \hat{J}(\mathbf{r}) \hat{A}(\mathbf{r}) dS, \tag{7}$$

where δA is the vector potential created by δJ. The second term of Eq. (7) is δJ independent and it is irrelevant to the minimization of $\mathcal{F}$. Then, minimizing $\mathcal{F}$ is equivalent to minimizing $\mathcal{F}'$, defined as

$$\mathcal{F}'[\delta J] \equiv \tfrac{1}{2} \int_S \delta J(\mathbf{r}) \delta A(\mathbf{r}) dS. \tag{8}$$

To compare the minimization of $\mathcal{F}'$ at every time layer with that for W' for the final J reached from the virgin state, we do the following. Given a physical J, we divide it into n terms δJ_i, so that $J(\mathbf{r}) = \Sigma_{i=1}^{n} \delta J_i(\mathbf{r})$, being n is a large number. We choose these terms as the actual current density incre-

ments in the virgin curve corresponding to the time layer at $t=t_i$, $\delta J_i=\delta J(t=t_i)$ with $t_i>t_{i-1}$. If the current penetrates monotonically, all δJ_i enclose a field-free region, or core. Furthermore, if n is very high δJ_i is nonzero in a thin layer only, so that δA_i created by δJ_i is almost uniform in the layer and

$$\mathcal{F}'[\delta J_i]=\tfrac{1}{2}\int_S \delta J_i \delta A_i dS \approx \tfrac{1}{2}\delta A_{i,c}(I_i-I_{i-1}), \tag{9}$$

where $\delta A_{i,c}$ is the vector potential in the field-free core created by δJ_i and I_i is $I(t_i)$, with $I(t_0)=0$.

From Eqs. (5) and (2) and using the same division, we can separate W' as

$$W'[J]=\tfrac{1}{2}\int_S (J-\delta J_1)(A-\delta A_1)dS+\tfrac{1}{2}\int_S \delta J_1\delta A_1 dS+\int_S (J-\delta J_1)\delta A_1 dS, \tag{10}$$

where δJ_1 is the first increment of supercurrent density set in the superconductor. Since the current set after δJ_1 lies inside the field-free core corresponding to δJ_1, the last term in Eq. (10) follows $\int_S(J-\delta J_1)\delta A_1 dS=\delta A_{1,c}(I-I_1)$. Inserting this into Eq. (10) and using Eq. (9) we obtain

$$W'[J]\approx \tfrac{1}{2}\int_S (J-\delta J_1)(A-\delta A_1)dS+\delta A_{1,c}[I-I_1/2]. \tag{11}$$

Following the same steps for all δJ_i, we find that

$$W'[J]\approx \sum_{i=1}^{n}\delta A_{i,c}[I-(I_i+I_{i-1})/2]. \tag{12}$$

At this point we notice that when minimizing $\mathcal{F}'[\delta J_i]$ for each time layer, each $\delta A_{i,c}$ is minimized [Eq. (9)]. From Eq. (12) we see that, since I_i are fixed external parameters, minimizing all $\delta A_{i,c}$ leads to minimizing W'. If the δJ_i which minimizes $\mathcal{F}'[\delta J_i]$ is unique, the $J=\Sigma_{i=1}^{n}\delta J_i$ minimizing W' is also unique. Then, if we are only interested in the final J, it can be obtained by minimizing directly W' by means of any minimization routine.

The assumption of monotonic penetration of current in the initial curve is consistent with our numerical results for arrays of strips connected in parallel (Figs. 1, 6, and 14), our preceding results for cylinders and single strips[24,32,34,36] and the analytical solution for a double thin strip in Ref. 18, Fig. 14.

C. Calculation of current distribution

The current distribution in the whole alternating current cycle can be deduced from the current profiles for the states on the initial curve, provided that the current penetrates monotonically when the state evolves along this curve as the present case. Let us consider first the reversal curve, for which I monotonically decreases from I_m to $-I_m$. We note that $\mathcal{F}'$ in Eq. (8) remains unchanged if we reverse the sign of δJ. Then, if on the initial curve $\mathcal{F}'$ in Eq. (8) is minimized when current with $J=J_c$ monotonically penetrates from the surface inwards, in the reversal curve $\mathcal{F}'$ is minimized when new current with $J=-J_c$ penetrates in the same way as for the initial curve. From these considerations, one can directly find that $J_{\rm rev}(I)=J_{\rm in}(I_m)-2J_{\rm in}[(I_m-I)/2]$, where $J_{\rm rev}$ and $J_{\rm in}$ are the current density on the reverse and initial curve, respectively. Following the same discussion for the returning curve ($I=-I_m$ to $I=I_m$), we obtain that the current density $J_{\rm ret}$ on this curve is $J_{\rm ret}(I)=J_{\rm in}(I_m)-2J_{\rm in}[(I_m-I)/2]$, closing the current cycle. This result was already found for single strips in Refs. 15 and 43.

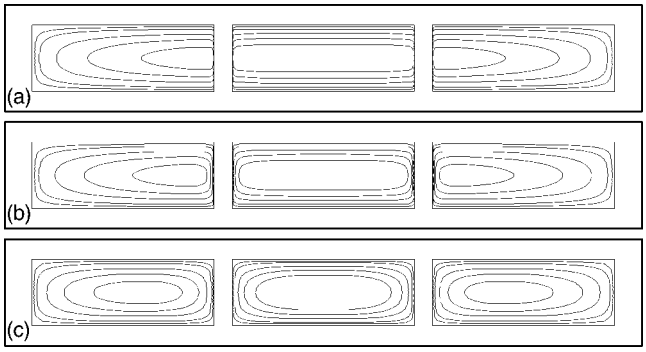

FIG. 1. Current fronts for horizontal arrays made of three strips with aspect ratio $a/b=20$ and separations $d_x/a=0.02$ (a), 0.2 (b), and 4 (c). The current fronts correspond to $I/I_c=0.1$, 0.2, 0.4, 0.6, and 0.8 from outer to inner. The vertical axis has been expanded and strip separations have been drawn as the same for better visualization.

We now describe how we calculate the current distribution for a certain current I starting from the zero-field cooled state by means of MEM.

Each superconducting strip is divided into $N=2n_x\times 2n_y$ elements with dimensions $a/n_x\times b/n_y$; current density is assumed to be uniform in each element. We allow the current density to have discrete values below J_c, that is, $J=mJ_c/m_m$ with m being an integer number from 1 to a maximum value m_m. As discussed in Ref. 24, the allowance of current densities lower than J_c reduces the discretization error in the ac loss calculation. Actually, we find that a value of J smaller than J_c appears only within one layer of elements beyond the $J=J_c$ front. This layer simulates much better the effect of a smoothly curved front.

We consider an already present numerical profile which minimizes the internal energy with a total current I. Then, we increase the current for $\Delta I=J_c ab/n_x n_y m_m$ in the nonsaturated element where doing so increases the least the internal energy; I is therefore increased to $I+\Delta I$ and internal energy is kept as the minimum possible. This procedure is repeated from $I=0$ up to $I=I_c$, obtaining all the profiles at a discretized set of I values in the process.

The variation of W', $\Delta W'$, as a consequence of changing the current in element l, from I_l to $I_l+\Delta I$ can be calculated from Eq. (5) as

$$\Delta W'=\sum_{j=1}^{N} C_{jl}I_j\Delta I+\tfrac{1}{2}C_{ll}(\Delta I)^2, \tag{13}$$

where the factors C_{jl} are defined as the vector potential created by unit current in element j averaged over the cross

section of element l. These factors can be calculated analytically and are presented in the Appendix.

D. Calculation of ac loss

For constant J_c and monotonic current penetration, the transport ac loss per cycle, Q, at current amplitude I_m can be directly calculated from the current profile at $I=I_m$ as[15]

$$Q = 4\int_S J(\mathbf{r})\Phi(\mathbf{r})dS, \tag{14}$$

where $\Phi(\mathbf{r})$ is the magnetic flux per unit length between the flux-free core and position $\mathbf{r}$. Using $\mathbf{B}=\nabla\times\mathbf{A}$ and the Stokes theorem, one obtains that $\Phi(\mathbf{r})$ equals the vector potential difference between the flux-free core and position $\mathbf{r}$. Considering this and taking into account that the vector potential generated by the returning tape is practically uniform in the tape at the origin, we deduce from Eq. (14) that

$$Q = 4\int_S J(\mathbf{r})[A_c - A(\mathbf{r})]dS, \tag{15}$$

where A_c is the vector potential in the flux-free core.

The evaluation of Q from the numerical current profile yields to

$$Q = 4\left[I_m\sum_{j=1}^{N} A^j(\mathbf{r}_c) - \sum_{j,l=1}^{N} C_{jl}I_jI_k \right], \tag{16}$$

where A^j is the vector potential due to the element j and $\mathbf{r}_c$ is a position inside the core. Analytical expressions for $A^j(\mathbf{r})$ can be found in the Appendix.

To calculate the loss for I_m up to I_c it is necessary to know the kernel position. The kernel is defined as the last point to be penetrated by current in the initial curve, so that it always belongs to the field-free core for any $I_m \leqslant I_c$. For a matrix array with odd $n_{s,x}$ and $n_{s,y}$ the kernel is always located at the center due to the mirror symmetry, but for even $n_{s,x}$ and/or $n_{s,y}$ the determination of the kernel is not obvious. Since $\mathbf{B}=0$ always in the kernel, its position can be found as the point where $\mathbf{B}=0$ inside the superconducting region when $I=I_c$. After calculating the magnetic induction generated by a saturated rectangular strip using the Biot-Savart law, the kernel position can be found numerically using the Newton-Raphson method for nonlinear systems of equations.[44] Due to symmetry, for matrices with one of $n_{s,x}$ and $n_{s,y}$ to be even there appear two kernels in the two strips closest to the center, while when both $n_{s,x}$ and n_{sy} are even the system has four equivalent kernels.

III. RESULTS AND DISCUSSION

Although the numerical model presented earlier can be applied to any superconducting geometry with translational symmetry, in the present paper we restrict our study to regular arrays of rectangular strips. The behavior of the array will depend upon the magnetic interaction between strips. In order to analyze this behavior we will first make a systematic study of the magnetic interaction among rectangular strips in both horizontal and vertical arrays, and after that we will use such a study as a basis to the case of a matrix array. (Actually, in the transport case the results are independent of the array orientation so that a horizontal array of strips with dimensions a and b has exactly the same properties as a vertical one with strips with dimensions b and a; for clarity of exposition, we will refer to horizontal or vertical arrays because we will always consider strips with $a/b \geqslant 1$, so a horizontal array of strips will consist of strips aligned in the direction perpendicular to their short dimension, and a vertical array arranged in the parallel direction.)

A. Horizontal arrays

1. Dependence on strip separation

To illustrate the current penetration process in a horizontal array, we show the calculated current profiles for different values of current for a three-strip horizontal array with dimensions $a/b=20$ and $d_x/a=0.02$, 0.2, and 4 in Figs. 1(a)–1(c), respectively. The arrays are artificially drawn with the same separation to facilitate the profiles' comparison.

The general observed behavior is that current penetrates from the superconductor borders inwards, being the penetration deeper from the external vertical border of the side strips, so that the current carried by the side strips is higher. The current profiles for lower d_x/a, Figs. 1(a) and 1(b), do not differ significantly from those obtained as if the array were a single strip with the overall dimensions, except near the strip gaps for the case $d_x/a=0.2$, Fig. 1(b). When d_x/a increases [Fig. 1(c)], the current penetration from the inner boundaries is enhanced and the field-free core in the side strips moves towards the strip center. Moreover, the current fraction carried by each strip in the array becomes more similar to each other with increasing d_x/a. Then, the current profiles for the large d_x/a limit would be identical for all the strips and equal to those for each of the superconducting strips taken independently.

We notice that the high d_x/a limit is reached much slower for the transport case than for the magnetic one, that is, for arrays of strips under a uniform applied ac field.[33] This is because the magnetostatic coupling between strips has a longer range in the transport array than in the magnetic case; for the transport situation the field produced by a strip varies with distance r as $1/r$, while for the magnetic case the net current in a strip is zero so that its field, dominated by the dipolar contribution, varies as $1/r^2$.

In order to study the behavior of the magnetic field, in Fig. 2 we plot the vector potential difference $A_c-A(\mathbf{r})$ level curves and the current profile for a three-strip array with $a/b=20$ and $d_x/a=0.2$ [Fig. 2(a)] and $d_x/a=1$ [Fig. 2(b)] carrying a current $I=0.6I_c$. The presented A_c-A level curves can be either regarded as magnetic field lines[25,33] and also, in the region where $J_z=J_c$, as the ac loss density level curves. This latter property of A_c-A can be found from Eq. (15) considering that the only region where $0<J_z<J_c$ is a thin layer of one-element width surrounding the flux-free core,[24] where $A_c-A=0$. As expected from the current profiles in Fig. 1, results show that if the separation d_x/a is low enough [Fig. 2(a)], the vector potential, the magnetic field, and the current

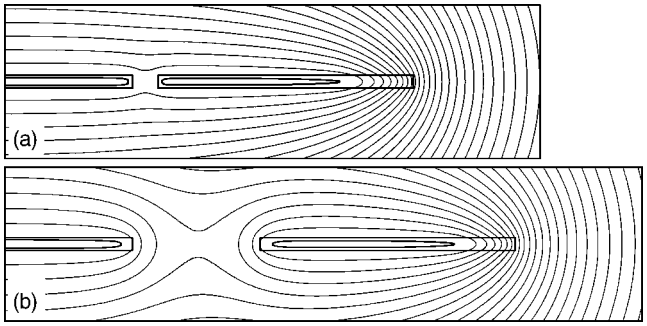

FIG. 2. Current fronts (thick lines) and magnetic flux lines [actually they are $A_c - A(\mathbf{r})$ level curves; see text] for horizontal arrays made of three strips with aspect ratio $a/b=20$ and separation $d_x/a=0.2$ (a) and $d_x/a=1$ (b) carrying a transport current $I=0.6I_c$. Only the right half part of the tape is plotted. The $A_c - A(\mathbf{r})$ variation between level curves is the same for both plots.

profile are very similar to those for a single strip with the overall dimensions. If d_x/a increases, Fig. 2(b), these electromagnetic quantities change progressively to approach those for magnetically uncoupled strips. Another important issue is that the magnetic field between strips is very small compared to the field next to the external lateral edges. It can also be seen that the magnetic flux between the field-free core of different strips is zero, as expected.

From the obtained current profiles, we can calculate the ac loss. The normalized ac loss $q \equiv 2\pi Q/\mu_0 I_c^2$ per cycle as a function of the reduced current amplitude $i \equiv I_m/I_c$ corresponding to a three-strip horizontal array with $a/b=20$ and several values of d_x/a is plotted in Fig. 3. The curves for one isolated strip with $a/b=20$ and the well-known cases of ellipses and thin strips[15] are also plotted for comparison. For all cases I_c is the total critical current for the specific geometry. The infinite separation case ($d_x/a=\infty$) for a set of $n_{s,x}=n$ aligned strips can be calculated from the curve for a single strip $q(i, n_{s,x}=1)$ as $q(i, n_{s,x}=n)=q(i, n_{s,x}=1)/n$, since for $d_x/a=\infty$ the strips do not interact with each other and $I_c(n_{s,x}=n)=nI_c(n_{s,x}=1)$. This ac loss reduction in the superconductor may also be obtained by ideal magnetic shielding of the filaments.[7]

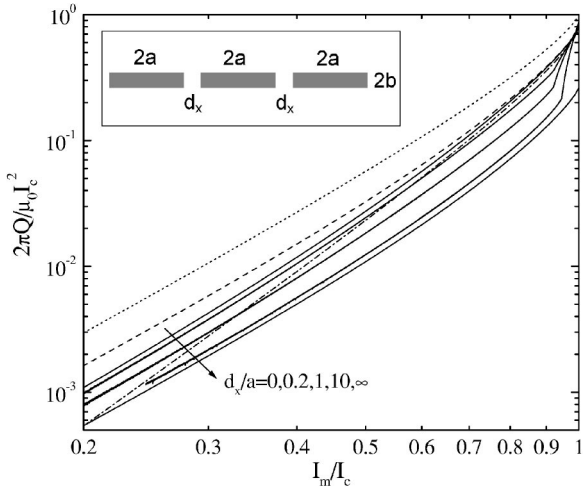

FIG. 3. Normalized ac loss $2\pi Q/\mu_0 I_c^2$ as a function of the normalized ac field amplitude I_m/I_c. Solid lines correspond to horizontal arrays made of three strips with $a/b=20$ and $d_x/a=0, 0.2, 1, 10, \infty$ in the arrow direction, the dashed curve to a rectangular strip with $a/b=20$, the dotted curve to the analytical formulas for ellipse (Ref. 15), and the dash-dotted curve to a thin strip (Ref. 15).

As it can be seen in Fig. 3, the curves for three-strip arrays present a sudden increase in the slope at a certain i value between 0.9 and 1, which corresponds to the full penetration of side strips. This effect can be explained as follows. The vector potential difference, and so the ac loss density, increases in magnitude from the field-free core outwards (Fig. 2). Since beyond the kink the only field-free zone belongs to the central strip, the ac loss density in the side strips increases more for the same current increment. Consequently, this slope increment is higher for larger strip separation, as shown in Fig. 3. The presence of a kink has also been found for geometries with discontinuities of the J_c value in the cross section.[16,45] It is also remarkable that the ac loss decreases when the strip separation increases for any i below 0.97. Furthermore, all calculated curves for nonzero d_x/a lay below the Norris strip curve for $i<0.97$ and $i>0.57, 0.34, 0.24, 0.20$ for $d_x/a=0.2, 1, 10, \infty$, respectively. The ac loss decreases with increasing the strip separation for i below the kink due to the decrease in the magnetic interaction with increasing the separation. This yields to a more similar current carried by each strip and a current profile more symmetric with respect to each strip midplane (Fig. 1). Then, since the vector potential decreases with the distance to the field-free core, the average vector potential difference $A_c - A$ in each strip is lower, as can be seen in Fig. 2, where the $A_c - A$ level curves are plotted.

Another interesting issue is that the normalized ac loss for a horizontal array of strips with $a/b \geq 1$ and i below the kink is lower than that for one of the strips taken independently for any d_x/a. This is so because the normalized ac loss q for a strip monotonically decreases with increasing a/b,[20,23,24] so that q for one of the strips is higher than for the horizontal array with $d_x/a=0$ and, consequently, higher for any d_x/a since magnetic coupling decreases with increasing d_x.

All the features discussed in this section are general for any horizontal array, as checked by numerical calculations.

2. Dependence on strip number

The current penetration profiles for different values of current in two horizontal arrays with two and nine strips and $a/b=20$ and $d_x/a=0.2$ are plotted in Figs. 4(a) and 4(b), respectively. The profiles corresponding to the two largest values of current ($I/I_c=0.8$ and 0.9) are depicted in dashed lines to help the profiles identification. For the array with two strips in Fig. 4(a) one of the array kernels is represented as a cross. An interesting feature of the profiles for the case of a large number of strips [such as $n_{s,x}=9$ in Fig. 4(b)] is that some of the strips are fully penetrated by currents even though $I/I_c<1$.

The normalized ac loss q as a function of i for different $n_{s,x}$ is plotted in Fig. 5. As expected, the $q(i)$ curves present several kinks; specifically, they present $(n_{s,x}-1)/2$ kinks if $n_{s,x}$ is odd and $(n_{s,x}-2)/2$ if $n_{s,x}$ is even, so that each kink

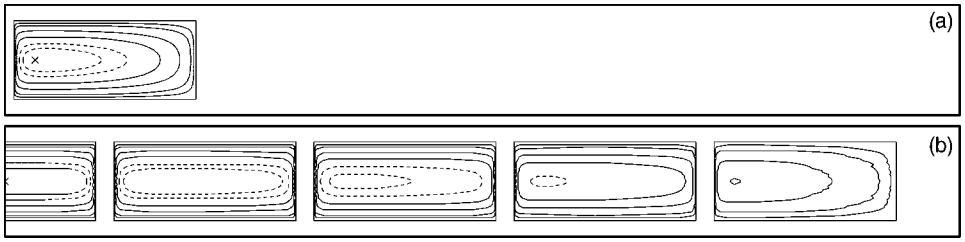

FIG. 4. Current fronts for horizontal arrays with $n_{s,x}=2$ (a) and 9 (b). Current profiles correspond to $i=0.1, 0.2, 0.4, 0.6$ (solid lines) and $i=0.8, 0.9$ (dash lines) from outer to inner. The cross shows the kernel position. Only the right half is plotted for space reasons.

corresponds to the full penetration of a pair of strips located symmetrically to the *zy* plane. Several other features can be discussed.

First, the lowest loss at $i=1$ is for $n_{s,x}=2$. This is so because linear arrays with even $n_{s,x}$ have two kernels, so that the average distance from a kernel to the current distribution, and so the vector potential difference, is lower than for any odd number, including $n_{s,x}=1$. Arrays with a higher even number of strips have a higher average distance from the kernels, so that $q(i=1)$ is higher.

Second, the normalized ac loss for low i is lower for higher number of strips. As it is explained later, this fact occurs when i is lower than the normalized current at which the most external strip is fully penetrated. Below this current, each strip is nonsaturated with current density penetrating from the whole strip contour, including the border next to the gap (Fig. 4). Since for higher $n_{s,x}$ there is a total larger interface between the field-free core and the critical-current density region, the average vector potential difference is lower, and so is the ac loss. After some strips become fully penetrated, so that the field-free core disappears from these strips, the ac loss increases faster with i. Then, the $q(i)$ curves for higher $n_{s,x}$ progressively overcome those for lower $n_{s,x}$. An important consequence of this is that the optimum number of strips regarding the normalized ac loss depends on the reduced current at which the array is desired to operate.

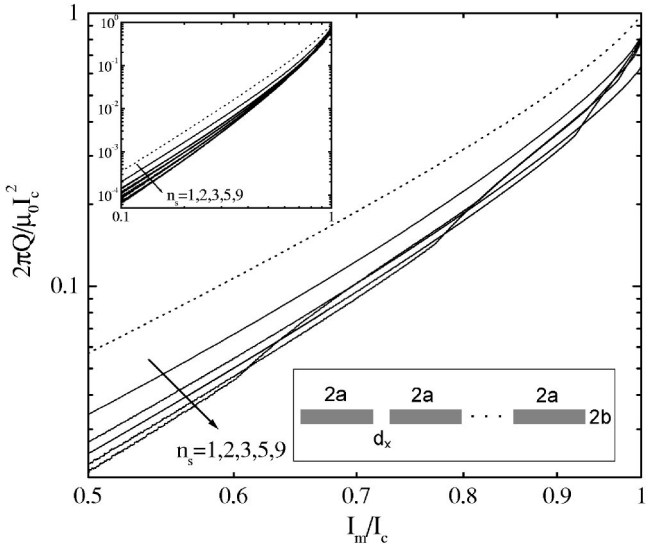

FIG. 5. Normalized ac loss $2\pi Q/\mu_0 I_c^2$ as a function of the normalized ac field amplitude I_m/I_c. Solid lines correspond to horizontal arrays with $a/b=20$, $d_x/a=0.2$, and $n_{s,x}=1$, 2, 3, 5, and 9 in the arrow direction and the dotted line is for an ellipse (Ref. 15). Inset shows the ac loss for a wider range of normalized current amplitude.

B. Vertical arrays

1. Dependence on strip separation

To illustrate the current penetration process in a vertical array, we show the calculated current profiles for different values of current for a three-strip vertical array with $a/b=20$ and $d_y/a=0.2$, 2, and 4 in Figs. 6(a)–6(c). We find that current profiles for vertical arrays have all the characteristics described earlier for horizontal arrays, with the difference that the transition from the overall behavior to the independent strip one requires higher separations in this case.

Magnetic flux lines, as well as the current profiles, are plotted in Figs. 7(a) and 7(b) corresponding to a vertical array of three strips with $d_y/a=0.2$ and 2, respectively, carrying a transport current of $I=0.6I_c$. It can be seen that the vertical array needs a higher separation to magnetically decouple the strips. The magnetic shielding in the gap between strips [Fig. 7(b)] is much higher than for the horizontal array with the same strip separation (Fig. 2).

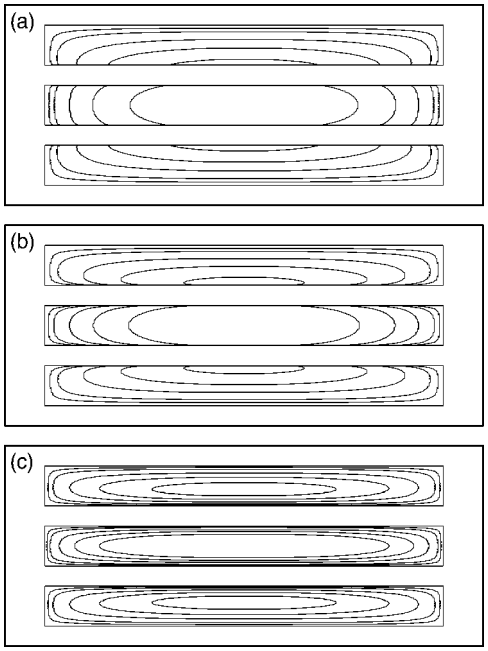

FIG. 6. Current fronts in vertical arrays made of three strips with aspect ratio $a/b=20$ and separations $d_y/a=0.02$, 0.2, and 4 (a,b,c). The current fronts correspond to $i=I_m/I_c=0.1$, 0.2, 0.4, 0.6, and 0.8 from outer to inner. The vertical axis has been expanded and strip separations have been drawn as the same for better visualization.

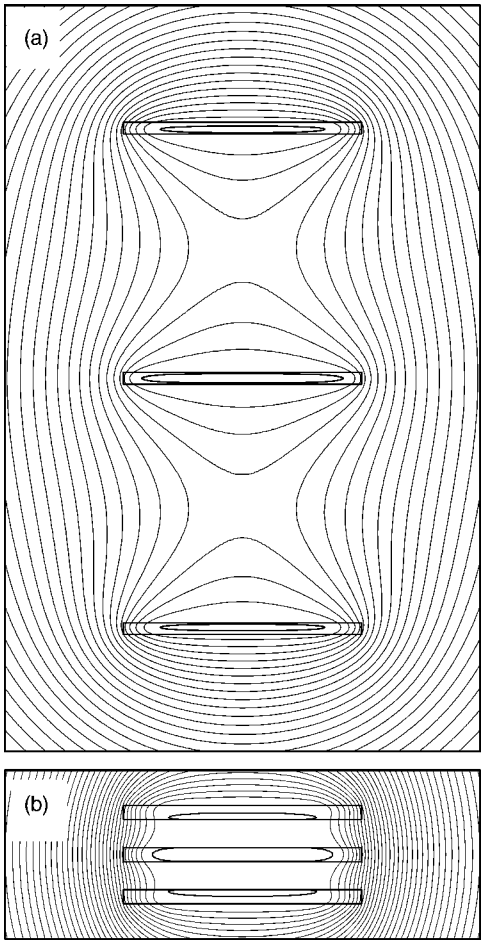

FIG. 7. Current fronts (thick lines) and $A_c - A(\mathbf{r})$ level curves as magnetic flux lines for vertical arrays made of three strips with aspect ratio $a/b=20$ and separation $d_y/a=1$ (a) and $d_x/a=0.2$ (b) carrying a transport current $I=0.6I_c$. The $A_c - A(\mathbf{r})$ variation between level curves for these figures is the same as for Fig. 2.

In Fig. 8 we present q as a function of i for vertical arrays with $n_{s,y}=3$, $a/b=20$, and several values of vertical separation d_y/a. As for horizontal arrays, the normalized ac loss for vertical arrays shows a kink between $i=0.9$ and 1 and below the kink it monotonically decreases with increasing strip separation. However, vertical arrays with small separation d_y/a present a higher loss than for one strip, although the lowest loss is still for vertical arrays with enough high d_y/a. The reason is simply because each strip has an aspect ratio a/b larger than the vertical array with no separation, so that the latter has a higher loss than the former.[20,23,24] However, with increasing d_y/a the loss below the kink decreases down to $1/n_{s,y}$ times the loss for one strip (Sec. III A 1). We note that the loss for a densely piled vertical array (small d_y/a) is more similar to that for a strip with a thickness equal to the sum of the superconducting region thickness than for a strip with the overall dimensions (superconducting volume plus air gaps). Another interesting issue is that the loss for the array with $i=1$ is higher than for a single strip for all the calculated d_y/a.

Numerical calculations have been performed for other a/b values, showing that all the earlier described trends and

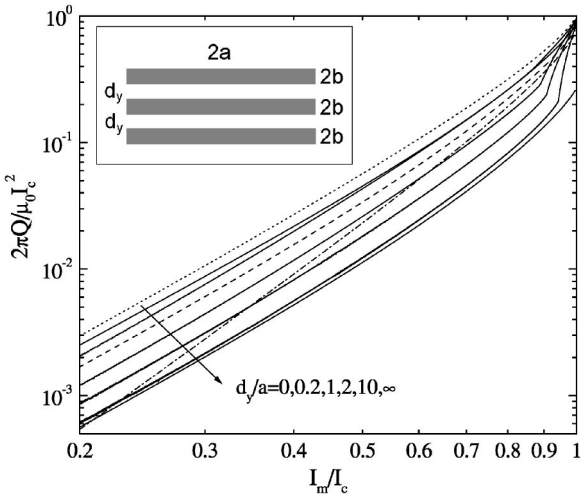

FIG. 8. Normalized ac loss $2\pi Q/\mu_0 I_c^2$ as a function of I_m/I_c. Solid lines correspond to a vertical array made of three strips with $a/b=20$ and $d_y/a=0,0.2,1,10,\infty$ in the arrow direction, the dash curve to a rectangular strip with $a/b=20$, the dot one to the analytical formula for ellipse (Ref. 15), and the dash-dotted curve to a thin strip (Ref. 15).

issues hold as long as $a/b \leqslant 20$. However, the case for higher aspect ratios is qualitatively different for low d_y/a. In Fig. 9 we present the $q(i)$ curves for a vertical array with $a/b=50$ and vertical separations $d_y/a=0$, 0.2, 2, and ∞, as well as the curve for one strip of the array. The only qualitative difference from Fig. 8 is that in Fig. 9 the normalized loss for $d_y/a=0.2$ is higher than that for $d_y/a=0$ when $i \geqslant 0.35$, while the kink is at much higher current. The reason for this reversed trend for high a/b can be understood by means of

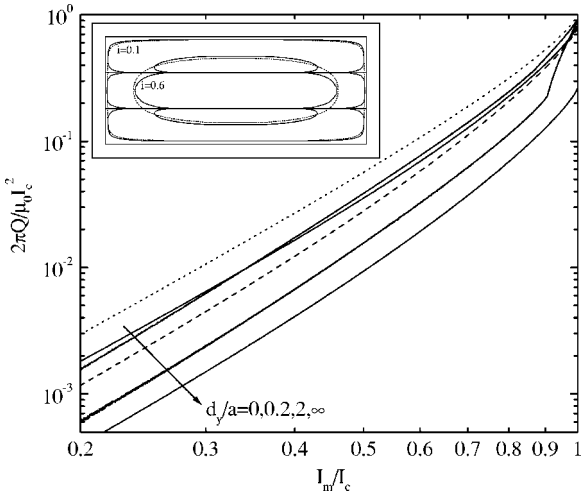

FIG. 9. Normalized ac loss as a function of normalized current amplitude. Solid lines correspond to a vertical array made of three strips with $a/b=50$ and $d_y/a=0,0.2,2,\infty$ in the arrow direction, the dashed curve to a rectangular strip with $a/b=50$, and the dotted curve to an ellipse. The inset shows the current fronts for a vertical array with $a/b=50$ and $d_y/a=0.2$ (solid lines) and a rectangular strip with $a/b=50/3$ (dotted lines). The strip separation for the array has been removed and the vertical axis has been expanded for better visualization.

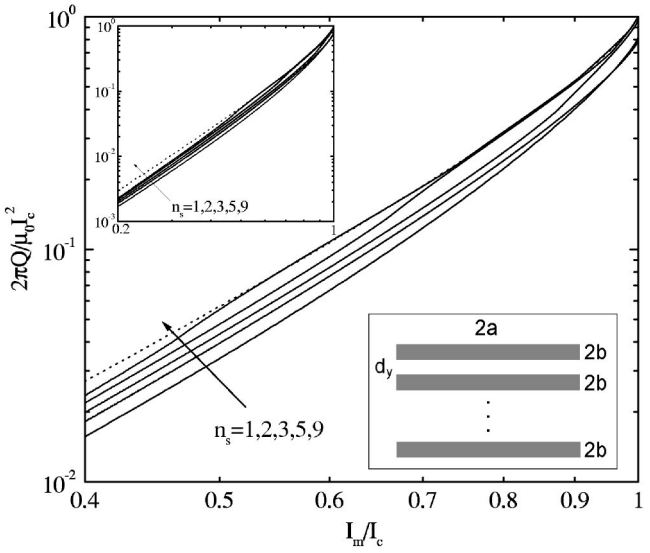

FIG. 10. Normalized ac loss as a function of normalized current amplitude. Solid lines correspond to vertical arrays of strips with $a/b=20$, $d_y/a=0.2$, and $n_{s,y}=1,2,3,5,9$ in the arrow direction and the dotted curve is for an ellipse. The inset shows the ac loss for a wider range of normalized current amplitude.

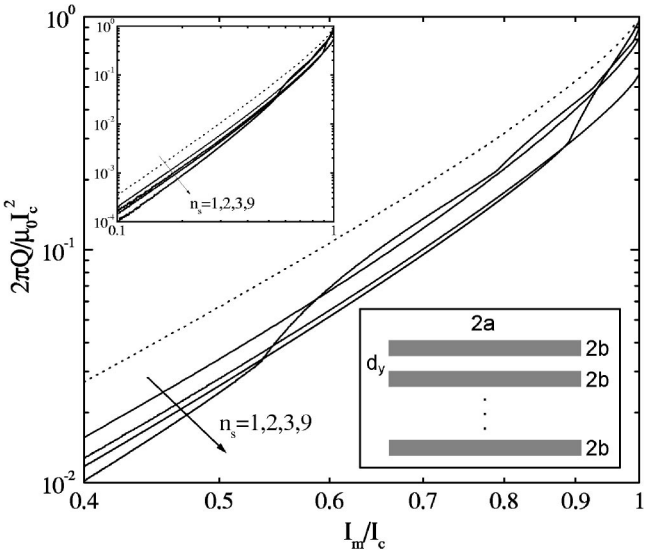

FIG. 11. Normalized ac loss as a function of normalized current amplitude. Solid lines correspond to vertical arrays of strips with $a/b=20$, $d_y/a=1$, and $n_{s,y}=1,2,3,9$ in the arrow direction and the dotted curve is for an ellipse. The inset shows the ac loss for a wider range of normalized current amplitude.

Fig. 9 (inset), where the current profiles for the above mentioned cases and $i=0.1$ and 0.6 are shown. The strips are depicted with zero separation to help the comparison. For vertical arrays with low d_y/a, the highest loss contribution comes from the current next to the outer vertical borders and the four most external corners [Fig. 7(b)], being the contribution of the current between the core and the gaps very small; this effect is enhanced for high a/b. For $i=0.1$, the case with $d_y/a=0$ has deeper current penetration from the four most external corners and the vertical borders than for $d_y/a=0.2$, so that the loss for zero separation is higher, whereas the opposite occurs for $i=0.6$. Then, the loss for low current is lower for $d_y/a=0.2$ than for zero separation, although for enough high current the loss for $d_y/a=0.2$ overcomes that for $d_y/a=0$ as shown in Fig. 9.

2. Dependence on strip number

We will study first the effect of stacking strips with low separation. In Fig. 10 we show the normalized ac loss for vertical arrays with $a/b=20$, $d_y/a=0.2$, and a different numbers of strips. It can be seen that $q(i)$ increases with increasing the number of strips. This is so because when d_y/a is low enough the array almost behaves as a single strip with aspect ratio $a/(n_{s,y}b)$ (Sec. III B 1); we call it the equivalent strip. Then, when increasing the number of strips, the equivalent strip aspect ratio decreases and the loss increases.[24] However, if the number of strips is so high that $a/(n_{s,y}b)<1$, this trend would be reversed since the loss for the equivalent strip is the same as if its aspect ratio is $n_{s,y}b/a>1$ and the transport ac loss do not depend on the overall orientation.

We see in Fig. 8 for $n_{f,y}=3$ that the ac loss of the array with $d_y/a=0.2$ is lower than that for $d_y/a=0$ when i is below the kink but it is the opposite at larger i. Such a behavior at low i has been confirmed for all the calculated cases of $n_{s,y}=2,3,5,9$ with the difference increasing with increasing $n_{s,y}$. This is so because for the same change in d_y/a the average distance between one strip and the rest of the strips increases more for higher number of strips, so that the magnetic interaction among the strips is more reduced compared with the case of $d_y/a=0$, where all the strips are incorporated into a single one with an aspect ratio of $a/(n_{s,y}b)$.

The normalized ac loss for arrays with the same strip aspect ratio, $a/b=20$, but larger vertical separation, $d_y/a=1$, is presented in Fig. 11 for several values of $n_{s,y}$. For this case, q decreases with $n_{s,y}$ for i below the lowest kink, being this trend is opposite to that for low d_y/a, Fig. 10. This trend appears when the strips are sufficiently magnetically decoupled, so that the governing aspect ratio comes from the strip itself but not from the overall. For higher i values, the outer strips subsequent penetration generates kinks in the $q(i)$ curve which yield a crossover between curves for several $n_{s,y}$, as already found for horizontal strips (Sec. III B 2).

C. Magnetic interaction in matrix arrays

In this section we study the electromagnetic interaction between rectangular strips arranged in a matrix configuration. In Fig. 12, we present the magnetic flux lines and current profiles for matrix arrays with $a/b=20$, $d_y/a=0.2$, and $d_x/a=0.2$ and 2 in Figs. 12(a) and 12(b), respectively. For both cases the reduced current is $I/I_c=0.6$ and the vector potential difference between flux lines is the same. As can be seen in Fig. 12, the current profile and magnetic flux lines present the same features as for horizontal and vertical arrays, Figs. 2 and 7(b).

The calculated ac loss for a $n_{s,x}\times n_{s,y}=3\times 3$ matrix array with $a/b=20$ and several values of d_x/a and d_y/a separations is shown in Fig. 13. In Fig. 13(a) we plot the $q(i)$

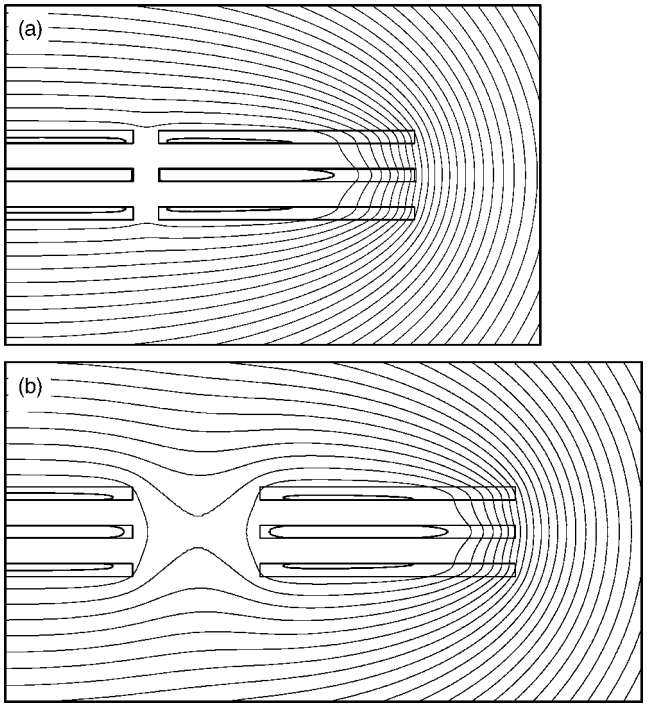

FIG. 12. Current fronts (thick lines) and $A_c - A(\mathbf{r})$ level curves as magnetic flux lines for a 3×3 matrix array of strips with aspect ratio $a/b=20$, $d_y/a=0.2$ and $d_x/a=0.2$ (a) and $d_x/a=1$ (b). In both cases the array carries a transport current $I=0.6I_c$. The $A_c - A(\mathbf{r})$ variation between level curves for both cases is the same.

curves for a fixed $d_y/a=0.2$ and several values of d_x/a. As expected after the discussion in Sec. III B 1, the normalized ac loss monotonically decreases with increasing d_x/a down to $1/n_{s,x}$ times the loss for a column taken independently. Moreover, the loss for low d_x/a is similar to that for a vertical array with a strip width equal to $2n_{s,x}a$. The loss results for the calculated case of $d_y/a=0.2$ and $d_x/a\leqslant0.2$ show that at small distances q may be well approximated by that of a strip made of all the strips in the array without distances. For arrays with overall width-to-thickness higher than 1, this approximation is more accurate than considering the loss of a strip with overall dimensions, especially for vertical distances of the order of the thickness of the stips.

The effect of varying the vertical distance between strips can be illustrated by the results shown in Fig. 13(b), where we plot the $q(i)$ curves for matrices with a fixed $d_x/a=0.2$ and several vertical distances d_y/a. The main features in this figure are the same as in Fig. 9. The kinks corresponding to the external strips penetration are clearly seen. The figure shows that the loss for low d_y/a slightly increases with vertical separation for $i\geqslant0.2$ and decreases for lower i, as can be seen from the slope at $i=0.2$. Compared to Fig. 9, this increase in q with increasing d_y/a for moderate i is enhanced since the electromagnetic behavior of each row is similar to that for a strip with aspect ratio $3a/b=60$, which is higher than a/b for Fig. 9. Considering a further increase of d_y/a, the loss gradually decreases down to $1/n_{s,y}$ times the loss for a horizontal array of $n_{s,x}$ strips due to the decrease in the magnetic coupling.

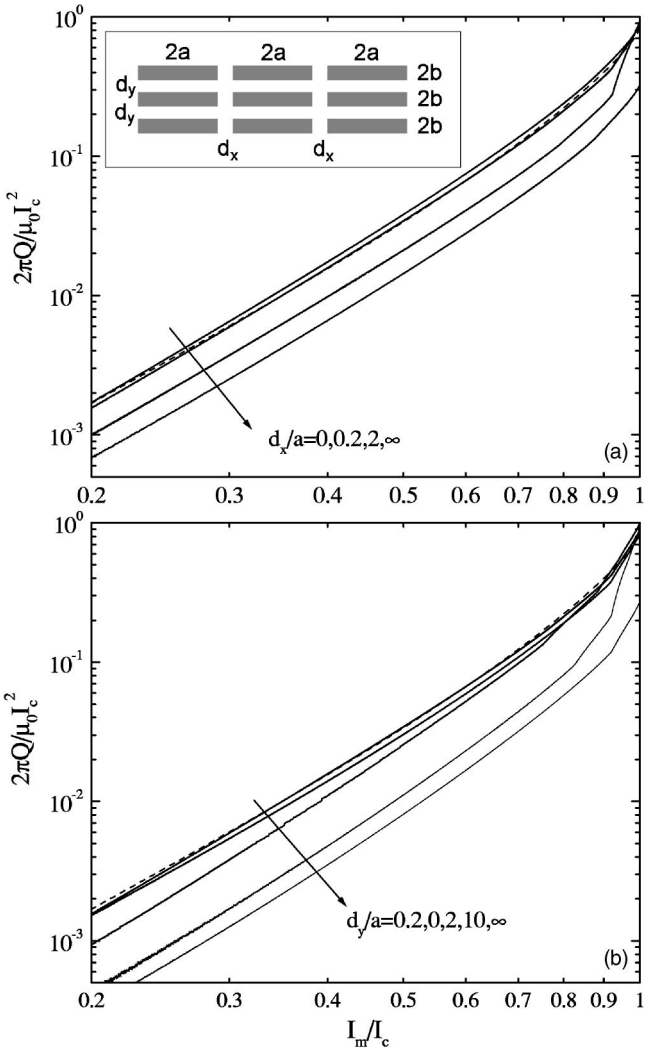

FIG. 13. Normalized ac loss as a function of normalized current amplitude. Solid lines correspond to a 3×3 matrix array of strips with $a/b=20$ and several strip separations. In (a) matrices have the same vertical separation $d_y/a=0.2$ and several horizontal ones $d_x/a=0,0.2,2,\infty$ in the arrow direction, whereas in (b) separations are $d_x/a=0.2$ and $d_y/a=0.2,0,2,\infty$ in the arrow direction.

D. Comparison with existing analytical limits and experimental results

1. Double thin strip

We present the sheet current density K (current density integrated over the thickness) for a two-strip horizontal array with $a/b=100$, $d_x/a=2$, and $d_x/a=0.2$ in Figs. 14(a) and 14(b), respectively, at several normalized current values. In both figures, solid lines correspond to our numerical calculations, while dashed lines are for the analytical solutions found by Ainbinder and Maksimova for a double thin strip.[18] As can be seen in the figure, the analytical profiles clearly agree with the numerical ones, which can be used as a check of our calculations.

2. Comparison with experimental data

Many experiments showed that the transport ac loss in multifilamentary tapes with densely packed filaments is very

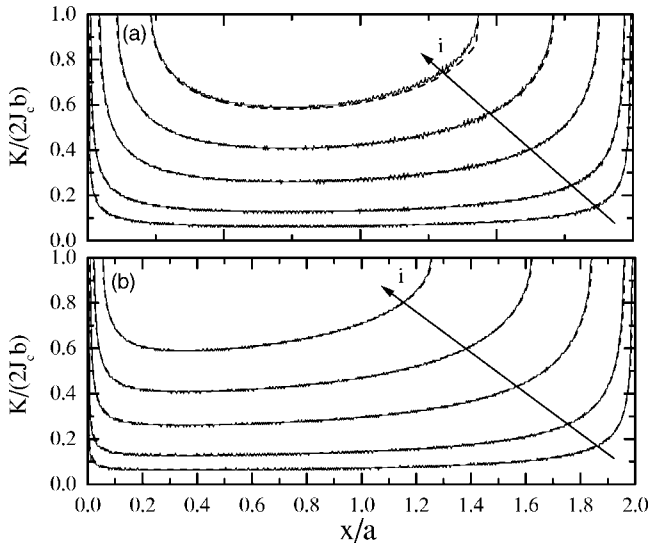

FIG. 14. Sheet current profiles for a horizontal array of two strips with $a/b=100$, $d_x/a=2$ (a) and $d_x/a=0.2$ (b), and $i=0.1$, 0.2, 0.4, 0.6, and 0.8 in the arrow direction. Solid lines correspond to our numerical results, while dashed lines correspond to the analytical formulas in Ref. 18 for a double thin strip.

similar to that for an ellipse or a thin strip, depending on the overall geometry,[6,46–48] being this effect consistent with the numerical data and discussion in Sec. III C.

More interesting is the measured ac loss for tapes with filaments in matrixlike arrangements, obtained by biaxial rolling. In Ref. 22 there is shown both experimental and numerical data for $Q(I)$ curves, which present a kink and are slightly lower than those for a thin strip for a certain current range. Some kinks in experimental data can also be seen in Ref. 29 for the 5×6 matrix curve with the lowest frequency. These experimental data are in agreement with the calculated results of Sec. III C.

The calculated data can also be compared to the experimental ac loss for two interacting tapes. In Refs. 9 and 11 it is shown that the ac loss of the interacting tapes, either arranged vertically or horizontally, decreases with the strip separation down to a half of the loss for an independent tape. A similar feature is observed in Ref. 10. This behavior is theoretically predicted in Secs. III B and III A for linear arrays of strips. Moreover, in Ref. 11 it is observed that when the two tapes are placed horizontally, the ac loss for low distances is lower than when they are placed vertically. As discussed in Secs. III A 1 and III B 1, this is due to the fact that arrays with low separation behave similarly to the overall, the horizontal array has a higher width-to-thickness aspect ratio and the loss for strips decreases with the aspect ratio.

IV. CONCLUSIONS

In this paper we have presented a numerical model to calculate electromagnetic properties of infinitely long superconductors in the critical-state model carrying a transport alternating current. The model has been applied to calculate the current profiles, the magnetic flux lines, and the ac loss for horizontal, vertical, and matrix arrays of rectangular strips with dimensions $2a\times2b$ assuming a constant critical-current density.

We have found that with increasing the strip distance, the current profile and the magnetic field progressively changes from the overall behavior to the uncoupled filament behavior, being this transition slower for vertical arrays. Moreover, the distance required to uncouple the strips is much higher for the transport case than when the array is immersed in a uniform ac field.

The normalized ac loss $q=2\pi Q/\mu_0 I_c^2$ as a function of the normalized current amplitude $i=I_m/I_c$ presents some kinks, which correspond to full penetration of the external strips. For horizontal arrays at i below the first kink, q decreases monotonically with increasing strip separation. This trend also holds for vertical and matrix arrays except for $n_{s,x}a/b>20$ and low horizontal and vertical separations, for which the trend is reversed for i above a certain value much lower than that of any kink. Furthermore, if the strip separation is high enough and i is not very low, the normalized ac loss can be significantly lower than that for the thin strip and, consequently, any single rectangular strip. Numerical results also show that when d_x/a and d_y/a are small enough ($d_x/a\leqslant0.2$ and $d_y/a\leqslant0.2$), the loss is close to that for a strip with aspect ratio $n_{s,x}a/n_{s,y}b$, being $n_{s,x}$ and $n_{s,y}$ the numbers of strips in the horizontal and vertical directions, respectively.

The effect of varying the number of strips in a horizontal or vertical array has been studied as well. For a horizontal array, the loss for i below the first kink decreases with increasing the number of strips, although for i above the first and subsequent kinks the loss for higher $n_{s,x}$ overcomes that for lower $n_{s,x}$. This is the same trend as for vertical arrays with high strip separation. However, for lower vertical separations, the loss monotonically increases with increasing $n_{s,y}$. Furthermore, the normalized loss for an even number of strips and i very close to 1 is lower than for an odd number of strips, being $q(i\simeq1)$ minimum for two strips.

Since many of the important issues such as magnetic coupling and finite size of the strips are incorporated in our model, the presented results may be used in the design of the filament arrangements in actual superconducting tapes in order to reduce the ac loss in them.

AKNOWLEDGMENTS

Financial support given by MCyT Project No. BFM2000-0001, CIRIT Project No. SGR2001-00189, CeRMAE, and DURSI from Generalitat de Catalunya is acknowledged.

APPENDIX

In this Appendix we calculate the vector potential generated by a current element $A_z^j(\mathbf{r})$ and the coefficients C_{jl} appearing in Eqs. (13) and (16) that are used for calculating the internal energy and the loss. The vector potential $A_z^j(\mathbf{r})$ is also used for calculating the magnetic flux lines.

Vector potential generated by a current element

Let us consider an infinite rectangular bar along the z direction, centered at the origin, dimensions $2t\times 2d$ in the x and y directions, respectively, and carrying a uniform current I. The vector potential in the gauge $\nabla\cdot\mathbf{A}=0$ generated by the bar is in the z direction and can be calculated from Eq. (2) as

$$A_{\mathrm{bar}}(x,y;t,d) = -\frac{\mu_0 I}{8\pi t d}[f(x-t,y-d) - f(x-t,y+d) - f(x+t,y-d) + f(x+t,y+d)], \tag{A1}$$

where the function $f(u,v)$ is defined as

$$f(u,v) = \frac{1}{2}\left[-3uv + uv\ln(u^2+v^2) + u^2\arctan\left(\frac{v}{u}\right) + v^2\arctan\left(\frac{u}{v}\right)\right]. \tag{A2}$$

Then, the vector potential generated by a current element is $A_z^j(\mathbf{r}) = A_{\mathrm{bar}}(x-x_j,y-y_j;a/n_x,b/n_y)$, where (x_j,y_j) is the central position of the element.

Calculation of coefficients C_{jl}

The coefficients C_{jl} are defined as the vector potential per unit current generated by the element j averaged in element l volume. It follows according to this definition:

$$C_{jl} = \frac{1}{4t_l d_l}\int_{x_l-x_j-t_l}^{x_l-x_j+t_l} dx \int_{y_l-y_j-d_l}^{y_l-y_j+d_l} dy\, A_{\mathrm{bar}}(x,y;t_j,d_j)/I_j, \tag{A3}$$

where (x_l,y_l) and (x_j,y_j) are the central positions of the elements, $2t_l\times 2d_l$ and $2t_j\times 2d_j$, their dimensions, and I_j is the current flowing through the element j. After inserting Eq. (A1) in Eq. (A3), we obtain by direct integration

$$C_{jl} = \frac{-\mu_0}{32\pi t_j t_l d_j d_l}[g(x_l-x_j+t_l,y_l-y_j+d_l;t_j,d_j) + g(x_l-x_j+t_l,y_l-y_j-d_l;t_j,d_j) - g(x_l-x_j-t_l,y_l-y_j+d_l;t_j,d_j) + g(x_l-x_j-t_l,y_l-y_j-d_l;t_j,d_j)], \tag{A4}$$

being $g(u,v;t',d')$ defined as

$$g(u,v;t',d') = F(u-t',v-d') - F(u-t',v+d') - F(u+t',v-d') + F(u+t',v+d') \tag{A5}$$

with

$$F(u',v') = -\frac{25}{48}u'^2v'^2 - \frac{1}{48}(v'^4+u'^2-6u'^2v'^2)\ln(u'^4+v'^2) + \frac{u'^3v'}{6}\arctan\left(\frac{v'}{u'}\right) + \frac{u'v'^3}{6}\arctan\left(\frac{u'}{v'}\right). \tag{A6}$$

We note that the coefficients fulfill the relation $C_{jl}=C_{lj}$. The validity of this relation can be easily justified by the fourfold integral obtained from inserting Eq. (2) in (A3).

[1] J. R. Hull, Rep. Prog. Phys. **66**, 1865 (2003).
[2] M. P. Oomen, R. Nanke, and M. Leghissa, Supercond. Sci. Technol. **16**, 339 (2003).
[3] D. Larbalestier, A. Gurevich, D. M. Feldmann, and A. Polyanskii, Nature (London) **414**, 368 (2001).
[4] A. P. Malozemoff, D. T. Verebelyi, S. Fleshler, D. Aized, and D. Yu, Physica C **386**, 424 (2003).
[5] L. Gherardi, F. Gömöry, R. Mele, and G. Coletta, Supercond. Sci. Technol. **10**, 909 (1997).
[6] C. M. Friend, S. A. Awan, L. Le Lay, S. Sali, and T. P. Beales, Physica C **279**, 145 (1997).
[7] M. Majoros, B. A. Glowacki, and A. M. Campbell, Physica C **334**, 129 (2000).
[8] A. Melini, R. Tebano, and R. Mele, Physica C **340**, 308 (2000).
[9] T. J. Hughes, Y. Yang, C. Beduz, and A. Power, IEEE Trans. Appl. Supercond. **9**, 774 (1999).
[10] S. Choi, D. Kim, W. Nah, J. Joo, J. Jung, and K. Ryu, Physica C **372–376**, 1746 (2002).
[11] T. J. Hughes, Y. Yang, C. Beduz, and A. Power, Physica C **310**, 187 (1998).
[12] C. P. Bean, Phys. Rev. Lett. **8**, 250 (1962).
[13] H. London, Phys. Lett. **6**, 162 (1963).
[14] R. Hancox, Proc. IEEE **113**, 1221 (1966).
[15] W. T. Norris, J. Phys. D **3**, 489 (1970).
[16] F. Gömöry and L. Gherardi, Physica C **280**, 151 (1997).
[17] K.-H. Müller, Physica C **289**, 123 (1997).
[18] R. M. Ainbinder and G. M. Maksimova, Supercond. Sci. Technol. **16**, 871 (2003).
[19] W. T. Norris, J. Phys. D **4**, 1358 (1971).
[20] T. Fukunaga, R. Inada, and A. Oota, Appl. Phys. Lett. **72**, 3362 (1998).
[21] T. Fukunaga, R. Inada, and A. Oota, IEEE Trans. Appl. Supercond. **9**, 1057 (1999).
[22] A. Oota, R. Inada, N. Inagaki, P. X. Zhang, and H. Fujimoto, Physica C **386**, 100 (2003).
[23] M. Däumling, Supercond. Sci. Technol. **11**, 590 (1998).
[24] E. Pardo, D.-X. Chen, A. Sanchez, and C. Navau, Supercond. Sci. Technol. **17**, 83 (2004).
[25] E. H. Brandt, Phys. Rev. B **54**, 4246 (1996).
[26] J. Rhyner, Physica C **310**, 42 (1998).
[27] T. Yazawa, J. J. Rabbers, B. ten Haken, H. H. J. ten Kate, and H. Maeda, J. Appl. Phys. **84**, 5652 (1998).
[28] S. Stavrev, B. Dutoit, and P. Lombard, Physica C **384**, 19 (2003); S. Stavrev, B. Dutoit, and F. Grilli, IEEE Trans. Appl. Supercond. **13**, 3807 (2003).
[29] M. Dhalle, A. Polcari, F. Marti, Y. B. Huang, G. Witz, and R. Flükiger, IEEE Trans. Appl. Supercond. **9**, 782 (1999).
[30] F. Gömöry, J. Souc, A. Laudis, P. Kovac, and I. Husek, Supercond. Sci. Technol. **13**, 1580 (2000).
[31] D.-X. Chen, E. Pardo, and A. Sanchez, Supercond. Sci. Technol.

17, 16 (2004).
[32] A. Sanchez and C. Navau, Phys. Rev. B **64**, 214506 (2001); C. Navau and A. Sanchez, Phys. Rev. B **64**, 214507 (2001).
[33] E. Pardo, A. Sanchez, and C. Navau, Phys. Rev. B **67**, 104517 (2003).
[34] A. Sanchez and C. Navau, Supercond. Sci. Technol. **14**, 444 (2001).
[35] F. Gömöry, R. Tebano, A. Sanchez, E. Pardo, C. Navau, I. Husek, F. Strycek, and P. Kovac, Supercond. Sci. Technol. **15**, 1311 (2002); E. Pardo, A. Sanchez, C. Navau, F. Gömöry, I. Husek, F. Strycek, R. Tebano, and P. Kovac, Physica C **372–376**, 1788 (2002).
[36] E. Pardo, D.-X. Chen, A. Sanchez, and C. Navau, Supercond. Sci. Technol. **17**, 537 (2004).
[37] L. D. Landau, E. M. Lifshitz, and L. P. Pitaevskii, *Electrodynamics of Continuous Media*, 2nd ed. (Pergamon Press, New York, 1984).
[38] W. J. Carr, Jr., Physica C **402**, 293 (2004).
[39] L. Prigozhin, J. Comput. Phys. **129**, 190 (1996).
[40] L. Prigozhin, IEEE Trans. Appl. Supercond. **7**, 3866 (1997).
[41] A. Badia and C. Lopez, Phys. Rev. Lett. **87** 127004 (2001); A. Badia and C. Lopez, Phys. Rev. B **65** 104514 (2002).
[42] P. Chaddah, Pramana, J. Phys. **36**, 353 (1991); K. V. Bhagwat, S. V. Nair, and P. Chaddah, Physica C **227**, 176 (1994).
[43] E. H. Brandt, Phys. Rev. B **48**, 12 893 (1993).
[44] W. H. Press, S. A. Teukolsky, W. T. Vetterling, and B. P. Flannery, *Numerical Recipes in Fortran 77*, 2nd ed. (Cambridge University Press, Cambridge, 1996).
[45] J. Lehtonen, M. Ahoranta, and R. Mikkonen, Physica C **372–376**, 1743 (2002).
[46] M. Majoros, L. Jansak, S. Zannella, F. Curcio, P. La Cascia, V. Ottoboni, C. M. Friend, L. Le Lay, B. A. Glowacki, and A. M. Campbell, Physica C **310**, 6 (1998).
[47] A. Oota, T. Fukunaga, M. Matsui, S. Yuhya, and M. Hiraoka, Physica C **249**, 157 (1995).
[48] F. Gömöry, L. Gherardi, R. Mele, D. Morin, and G. Crotti, Physica C **279**, 39 (1997).